INSTITUTE OF PHYSICS PUBLISHING PLASMA SOURCES SCIENCE AND TECHNOLOGY

Plasma Sources Sci. Technol. **14** (2005) 283–292 doi:10.1088/0963-0252/14/2/009

Control of nitrogen species in helicon plasmas

R F Boivin[1] **and E E Scime**[2]

[1] Department of Physics, Auburn University, Auburn, Alabama, 36849-5311, USA
[2] Department of Physics, West Virginia University, Morgantown, West Virginia, 26506-6315, USA

Received 12 September 2004
Published 8 March 2005
Online at stacks.iop.org/PSST/14/283

Abstract

There are several possible reactions for both growth and decomposition of GaN layers in stable plasma conditions. A greater understanding of the plasma processes involved in the creation of the different N_2 species is required before many growth related problems can be resolved. A plasma source capable of selecting different active nitrogen species could be used to study the different reactions related to the growth process. In this paper, we present a spectroscopic study of a helicon plasma source. Five different nitrogen species in the plasma are monitored, namely: N II (atomic ion), N I (atomic neutral), N_2^+ (molecular ion) and two different excited states of the N_2 molecule as a function of the filling pressure. We show that by simply changing one plasma parameter (operating pressure), the plasma undergoes a transformation from an essentially atomic nature at low pressure to a dominantly molecular nature at higher pressure. The line intensity variations as a function of electron temperature are consistent with expectations based on the published formation rates for each species.

1. Introduction

Plasma-assisted molecular beam epitaxy (PAMBE) is currently used for growing thin films of wide band gap semiconductors such as GaN [1–4]. Current PAMBE systems utilize a conventional molecular beam epitaxy (MBE) source to provide the Ga flux while commercial RF plasma sources (e.g. Oxford[1] and EPI[2]) are used to produce active nitrogen species. These sources typically produce a complex mixture of active nitrogen superimposed on a background of presumed inert molecular nitrogen [5]. The compositions of these mixtures are different for each source since they result from a complex interaction of the plasma created inside the source with both the aperture and the plasma cavity walls. This complex interaction makes any modelling of these sources an almost impossible task. Of great concern is the plasma interaction with the pyrolytic boron nitride aperture, which introduces a significant amount of boron into the growing layer, with as yet unknown consequences on the resulting film properties. It is generally accepted that Oxford sources produce primarily atomic nitrogen with significant fractions of molecular ions and an unknown quantity of neutral metastables [6–8]. In contrast, EPI sources have a greater conductance than Oxford sources and produce plasmas dominated by nitrogen molecular species with a significant flux of molecular metastables [5].

Determining the effects of various active nitrogen species on layer growth is complicated. Previous experiments [6–8] showed that neither one of these sources produced enough ionic nitrogen (N^+) to account for the growth rate, suggesting that growth is due to other nitrogen species. Furthermore, atomic nitrogen, which is abundantly produced by the Oxford source, is relatively inefficient for growing GaN since it requires ten atoms in the flux for each one incorporated in the deposited layer. In contrast, the EPI source configuration used produced significantly less atomic nitrogen and yet achieved three to five times larger growth rates (1.0–1.5 μm h^{-1} for the EPI source, 0.3μm h^{-1} for the Oxford source) [6–8]. These results, coupled with the preliminary observations of molecular metastables during characterization, suggest that metastable molecular nitrogen is the dominant active nitrogen species in EPI source plasmas. Recent experiments suggest that growth rates of the wide band gap semiconductor GaN in MBE systems depend strongly on the relative fractions of atomic nitrogen and metastable molecular nitrogen in the RF plasma source [6–8].

[1] Oxford Applied Research, Oxfordshire OX29 9SP, UK.
[2] EPI Vaccum Products, St Paul, Minnesota, USA.

Table 1. Competing processes during the growth of GaN. The vertical arrows indicate the loss of either N_2 or Ga from the film.

Growth reactions	Competition to growth
(I) $Ga + N_2^+ + e^- \rightarrow GaN + N^*$	(VI) $GaN \rightarrow Ga\uparrow + \frac{1}{2}N_2\uparrow$ (decomposition)
(II) $Ga + N_2^* \rightarrow GaN + N^*$	(VII) $Ga_{adsorbed} \rightarrow Ga\uparrow$ (desorption)
(III) $Ga + N \rightarrow GaN$	(VIII) $GaN + N \rightarrow Ga + N_2\uparrow$ or $Ga\uparrow + N_2\uparrow$
(IV) $Ga + N^* \rightarrow GaN$	(IX) $GaN + N^* \rightarrow Ga + N_2\uparrow$ or $Ga\uparrow + N_2\uparrow$
(V) $Ga + N^+ + e^- \rightarrow GaN$	(X) $GaN + N^+ + e^- \rightarrow Ga + N_2\uparrow$ or $Ga\uparrow + N_2\uparrow$

As shown in table 1 [6–8], there are several possible reactions for both growth and decomposition of GaN layers in stable plasma conditions. Of particular relevance is that the nitrogen atomic ion (N^+), metastable atomic nitrogen (N^*) and neutral atomic nitrogen (N) can all participate in the formation (reactions III, IV and V) as well as the decomposition of GaN layers (reactions VIII, IX and X). This may explain the relatively poor efficiency of atomic nitrogen species for growth. Meanwhile, molecular species (N_2^* and N_2^+) contribute directly to the formation of a GaN layer (reactions I and II) and at most only indirectly contribute to the decomposition of the GaN since each formation of GaN also generates a nitrogen atom (most likely in an excited state). The growth-detrimental reactions VI and VII occur independently of the dominant growth mechanism. While rate constants of these reactions are not well known, qualitative conclusions based on free energy considerations are possible. Both atomic and metastable molecular nitrogen contain significantly more energy than required for GaN formation [9]. Incorporation of atomic nitrogen releases this energy into the lattice where it can drive unfavourable reactions such as Ga desorption, GaN dissociation or point defect formation. In contrast, the excited molecule can incorporate one N atom into growing GaN while the other atom desorbs, carrying away the excess energy. This scenario suggests improved growth based on the presence of excited molecular nitrogen. Competition between growth, surface decomposition and adsorbed nitrogen capture may also limit the efficacy of atomic nitrogen. Such a situation would promote point defect formation, supported by the poor electrical properties of the GaN film produced by the Oxford source [6–8].

A greater understanding of the plasma processes involved in the creation of the different N_2 species is required before many growth related questions can be resolved. Obviously, the GaN growth rate and film quality are dependent on the active nitrogen species present at the substrate. A plasma source capable of selecting different active nitrogen species could be used to study the different reactions listed in table 1. By isolating specific reactions, insight into the different growing or growth-detrimental mechanisms associated with nitrogen active species would be obtained. Identification of the optimal growth conditions could lead to improved PAMBE system designs capable of faster growth of high quality GaN crystal.

In this paper, we suggest that a different type of RF source, namely a helicon plasma source, could provide significant advantages over typical 'black box' commercial sources. The major advantage of the helicon plasma source over commercial RF sources is that specific reactive nitrogen species for film growth can be selected by controlling the electron temperature (T_e) in the plasma. A second significant advantage is that the helicon source is potentially a much cleaner source since, unlike conventional RF sources or glow discharges, it has neither antenna nor plasma filtering aperture inside the chamber. A third advantage is the simplicity (and low cost) of the helicon plasma source. Finally, a fourth advantage is that relatively simple models appear to be able to predict which nitrogen species will be dominant for a given T_e.

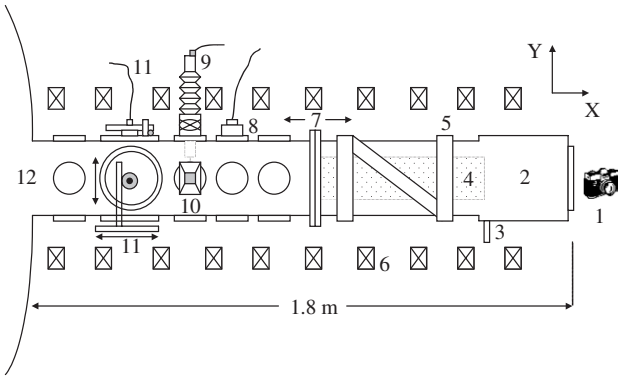

Figure 1. Upper view of the HELIX plasma source. (1) Digital camera (near axial viewport), (2) pumping station, (3) gas inlet, (4) plasma column, (5) fractional helix antenna, (6) magnetic field coils, (7) glass chamber section (right), SS chamber section (left), (8) spectroscopy optics, (9) retractable RF compensated Langmuir probe, (10) microwave interferometer, (11) two-dimensional LIF injection and collection optics, (12) large space chamber.

2. Experimental apparatus

The HELIX (Hot hELIcon eXperiment) helicon source generates steady-state plasmas in a 1.80 m long cylindrical vacuum chamber with a 0.15 m diameter. The present chamber is composed of two distinct sections: a glass section (0.60 m long) where the copper antenna wraps around the tube and couples RF radiation into the plasma and a metal section with ports distributed along its length for diagnostics (see figure 1). This metal section is in turn attached at one end to a large aluminium space chamber (4.5 m long, 2 m inner diameter). Three turbomolecular drag pumps with a total pumping speed of 3700 litre s^{-1} are connected to the vacuum chamber. The base pressure in the system is 2×10^{-8} Torr. Any gas or gas mixture can be injected through a feedback controlled piezoelectric valve. Typical operating gas pressures range from 0.1 to 50 mTorr. The steady-state HELIX magnetic field is generated with ten electromagnets that produce an axial magnetic field of 0–1300 Gauss [10]. A 0–50 MHz function generator supplies the RF signal to a steady-state RF amplifier. The amplifier can supply up to 2 kW of RF power over 0.3–30 MHz. The matching circuit is a standard π circuit consisting of four variable capacitors. The injected power is

limited by the quality of the match. An assortment of antennae can be used for experiments in HELIX: Nagoya type III [11], saddle coil [12] and fractional helical antenna [13]. For the experiments described in this paper, pure nitrogen plasmas are produced with a fractional helical antenna at 11 MHz. Other operating parameters such as filling pressure, magnetic field strength and RF power can be adjusted as needed to obtain the different N_2 species in the plasma.

The first reports of helicon experiments date from the late 1960s [12], but the mechanism responsible for the ionization efficiency of helicon sources is still not fully understood. One hypothesis [14, 15] is that resonant energy transfer between the helicon wave and electrons takes place in the plasma. While there are a number of interesting features unique to helicon sources, the most relevant to this proposal is their remarkable ionization efficiency. A second important feature is the flexibility of this type of source in terms of both operating pressure and gas mixture. Helicon sources can produce a variety of gas plasmas with electron densities in the 10^{10} to upper $10^{13}\,\mathrm{cm}^{-3}$ range and T_e between 3 and 20 eV [16]. A third significant feature is the absence of cathodes inside the chamber. Since the antenna is located outside the chamber there is no eroded or sputtered material in the plasma, contrary to what occurs in dc glow discharges and in most RF sources.

The HELIX helicon source produces within the 15 cm diameter glass tube a bright column of dense plasma (core, about 5 cm diameter) immediately bordered by a region of less intense radiation (core periphery, about 1.0 cm in length). The plasma is then surrounded by an annular region filled with neutral gas [16]. The column diameter varies slightly with the RF frequency, magnetic field strength and gas pressure [10]. The presence of that neutral layer around the column plays an important role in the recombination and quenching of the excited, ionized or dissociated molecules. Observations (digital camera) of the plasma column from a large viewport located at the front end of HELIX (see figure 1) indicate that the plasma is symmetrical around the central x-axis.

For the experiment described here, HELIX was instrumented with an extensive array of diagnostics located in the metal section of the chamber. These diagnostics include: a visible spectrometer, a radially scanning RF compensated Langmuir probe, a microwave interferometer and a laser induced fluorescence (LIF) diagnostic. The spectrometer is comprised of a Czerny–Turner 1.33 m scanning monochromator (wavelength range 185–1300 nm, holographic grating 1200 grooves mm^{-1}, F-number 11.6, dispersion $0.62\,\mathrm{nm\,mm}^{-1}$ and a maximum resolution of 0.015 nm) and, a charged coupled device (CCD) imaging camera (wavelength range 200–1100 nm, acquisition time from 10^{-2} s to several minutes, binning capability, 5.35 nm bandwidth and a quantum efficiency between 0.2 and 0.55 over the sensitivity range). The light collection system used a 25 mm collimator lens mated to a silica fibre optics cable with matching numerical aperture. The light collection unit is located 0.35 m downstream from the end of the antenna. The detection area defined by a light collection system at the centre of the plasma chamber is $0.07\,\mathrm{cm}^2$. A micro-positioning system is used to move the detection optics and a radial scan of the plasma column can be obtained. For any HELIX plasma conditions, photon count fluctuations represent $\approx$1% of the total integrated intensity except for low intensity lines (or bands) for which relative fluctuation can be as large as 5%.

Electron temperature (T_e) and plasma density (n_e) are measured by an RF compensated Langmuir probe. Basically, two modifications that have been made to a standard Langmuir probe [17, 18]. The first modification is the addition of a floating electrode. The electrode is exposed to the plasma potential fluctuations and is connected to the Langmuir probe tip via a capacitor. This helps to lower the sheath impedance and forces the Langmuir probe tip to follow the plasma potential oscillations, thereby reducing the distortion in the I–V trace. The second modification is a chain of RF chokes. These chokes are placed after the probe tip, but before current is measured. The Langmuir probe is connected to a high impedance source-meter that sweeps the voltage and records the collection current. The probe is located 0.15 m downstream from the optical window (0.50 m from the antenna). The probe is mounted on a 0.15 m translator with an integrated position vernier. A microwave interferometer, using direct measurements of phase shifts to determine the line-integrated electron density [19], is used to calibrate the Langmuir probe. The interferometer is located at exactly the same axial position as the Langmuir probe see figure 1.

Under the same steady-state plasma conditions, Langmuir probe I–V curves are very similar and yield almost identical T_e. Typically, T_e fluctuations are within 0.2 eV ($\approx$2%). The absolute uncertainty is more difficult to evaluate since the extraction of the T_e from the I–V curve is based on an approximate theory [20, 21]. Based on previous experiments with Langmuir probes in helicon plasma [10, 16, 18, 19, 22–25], we estimate the relative uncertainty in the T_e to be $\pm$15%. Plasma densities are evaluated by considering the ion saturation current section of the I–V curve (modified Langmuir equation or Allen equation [21, 26]). Density fluctuations within 5% are observed for all plasma conditions. Including uncertainties in the area of the probe, the microwave calibration, the T_e and in the ion saturation current measurement, the n_e uncertainty is within $\pm$15%.

3. Atomic processes in nitrogen plasma

The N_2 molecule has been extensively studied (see [27, 28]) because of the important role it plays in atmospheric phenomena, such as the aurora borealis as well as plasma processing. Typically, in helicon plasma conditions, electron collisions are primarily responsible for the creation of the different atomic and molecular species found in the plasma. T_e and n_e are the key parameters that determine the active N_2 species in plasmas. Furthermore, these parameters will, to a large extent, dictate the temperature of the N_2 species present in the plasma. As a first order approximation, electron impact cross-sections [29–32] for all the possible reactions can be used to estimate the relative abundance of each species.

3.1. Atomic and molecular species

The different reactions describing the important processes in N_2 helicon plasmas are listed as a function of increasing threshold energy (E_{th}) in table 2 [27, 33–35]. In helicon plasmas, the electron impact processes related to the

Table 2. Competing reactions in low temperature N_2 plasma.

Reactions	Threshold energy (eV)	Description
(1) $e^- + N_2 \rightarrow N_2^* + e^-$	6.17	Excitation (general)
(1a) $e^- + N_2 \rightarrow N_2^* (A\,^3\Sigma_u^+) + e^-$	6.17	Excitation ($A\,^3\Sigma_u^+$)
(2) $e^- + N_2 \rightarrow N(^4S) + N(^4S) + e^-$	9.80	Dissociation
(3) $e^- + N_2 \rightarrow N^* + N(^4S) + e^-$	12.14	Dissociative excitation
(3a) $e^- + N_2 \rightarrow N^*(^2D) + N(^4S) + e^-$	12.14	Dissociative excitation
(3b) $e^- + N_2 \rightarrow N^*(^2P) + N(^4S) + e^-$	14.34	Dissociative excitation
(4) $e^- + N \rightarrow N^+ + 2e^-$	14.55	Atomic ionization
(5) $e^- + N_2 \rightarrow N_2^+ + 2e^-$	15.58	Molecular ionization
(6) $e^- + N_2 \rightarrow N^+ + N(^4S) + e^-$	24.32	Dissociative ionization

vibrational excitation of the N_2 ground state $N_2(X\,^1\Sigma_g^+)$ are believed to be small when compared to the excitation processes described by reaction 1 (table 2). This is because the cross-sections for vibrational excitation processes peaks below 2 eV [29]. For $T_e \geqslant 3$ eV, the largest of these cross-sections $N_2(X\,^1\Sigma_g^+,\ \nu = 0 \rightarrow 1)$ is already more than 1 order of magnitude smaller than the cross-sections for the other excitation processes [29]. There are also strong indications that there is a significant flow of room temperature, vibrationally inert, N_2 gas in the helicon plasma core at all times. LIF measurements in the helicon plasma core using neutral rare gas species (He and Ar plasmas) have shown that neutrals are essentially at room temperature [36, 37]. For N_2 plasmas, room temperature neutrals would be incompatible with a large population the vibrationally excited N_2. Thus, we will assume in our first order model that all ground state N_2 are vibrationally inert within the plasma.

Reaction 1 corresponds to the electron excitation of the N_2 molecule to any neutral excited molecular state. The reaction cross-section corresponds to the total excitation cross-section involving the N_2 molecule (sum of the 10 largest excitation cross-sections for the N_2 molecule) [31, 38]. Reaction 1a corresponds to the excitation to the triplet molecular state $A\,^3\Sigma_u^+$, which is the first excited molecular level of the N_2 molecule. Reactions 2, 3 and 6 are associated with the break-up of the N_2 molecule into two nitrogen atoms. Reaction 2 results in the formation of two ground state atoms (^4S) [39], while 3a and 3b results in the formation of one metastable nitrogen atoms (^2D at 2.38 eV and ^2P at 3.58 eV above ground state) and one ground state N atom [40], respectively. Reaction 6 involves both the break-up and subsequent ionization of a nitrogen atom [41]. Reaction 5 describes the ionization of the nitrogen molecule, producing the molecular ion (N_2^+) [42]. Reaction 4 concerns the ionization of atomic nitrogen [43]. Except for reaction 4, all of these reactions result from electron collisions with the N_2 ground state, i.e. primary reactions. These processes are all statistically independent and their respective importance varies as a function of T_e. Reaction 4 is a secondary reaction since its reactant (N) is a product of reactions 2, 3 and 6. Reactions with even higher threshold energies (double ionization, dissociative ionization plus excitation, dissociative double ionization, stepwise excitation, etc) are not listed here since their respective magnitudes in low temperature plasmas are either unknown or negligible. Although these processes could be important under certain plasma conditions, we neglect them in this first order model. Other secondary processes related to the destruction of these newly created species (such as recombination and quenching) will be briefly discussed in sections 4 and 5.

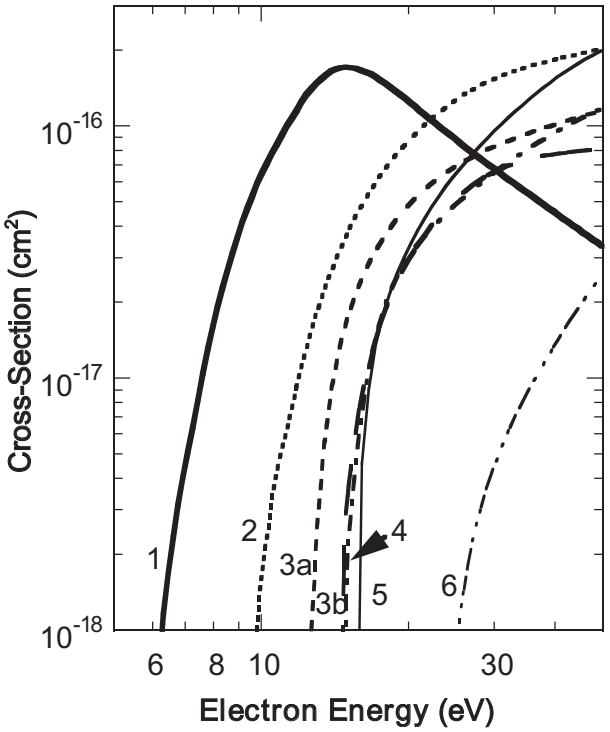

Figure 2. Cross-sections for the competing processes in low temperature N_2 plasmas. 1 (——) total excitation; 2 (· · · · · ·) N_2 dissociation; 3a (- - - -) dissociative excitation ^2D; 3b (— — —) dissociative excitation ^2P; 4 (— · —) atomic nitrogen ionization; 5 (——) molecular nitrogen ionization; 6 (— · · —) dissociative ionization.

The cross-sections for the different reactions (1, 2, 3a, 3b, 4, 5 and 6) are plotted in figure 2 as a function of electron energy. Excitation of the nitrogen molecule dominates at low electron energy, while dissociation processes as well as molecular ionization dominate at higher electron energy. These cross-sections are obtained from monoenergetic electron impact reactions. In plasmas, the different cross-sections must be averaged over the entire electron velocity distribution, yielding their respective rate coefficients. For these

calculations, we assume that the electron velocity distribution is described by a Maxwellian. The details of the electron velocity distribution in helicon sources are still a matter of considerable controversy. A number of groups have suggested that their experimental measurements indicate the presence of hot electrons [44–50]. Others have argued that the hot electron population is either very small compared to the thermal electron population or that no hot electrons are present during the steady-state operation of helicon devices [16, 51, 52]. Most relevant to this work is that a series of spectroscopy measurements performed on Ar helicon plasmas [51] clearly indicated that excitation rate coefficients calculated for a simple Maxwellian electron velocity distribution correctly described the plasma radiation. Therefore, we will assume that hot electrons represent at best a negligible fraction of the entire distribution and that the distribution is essentially Maxwellian. The rate coefficients for the different reactions are shown in figure 3 as function of T_e. The rate coefficients of the different reactions can be compared to determine which process is dominant in the plasma for a given T_e. In terms of formation rate (dA_i/dt, in $cm^{-3}\,s^{-1}$) we have [53]:

$$\frac{dA_i}{dt} = n_e n_{N_2} \langle \sigma \nu \rangle_i, \qquad (1)$$

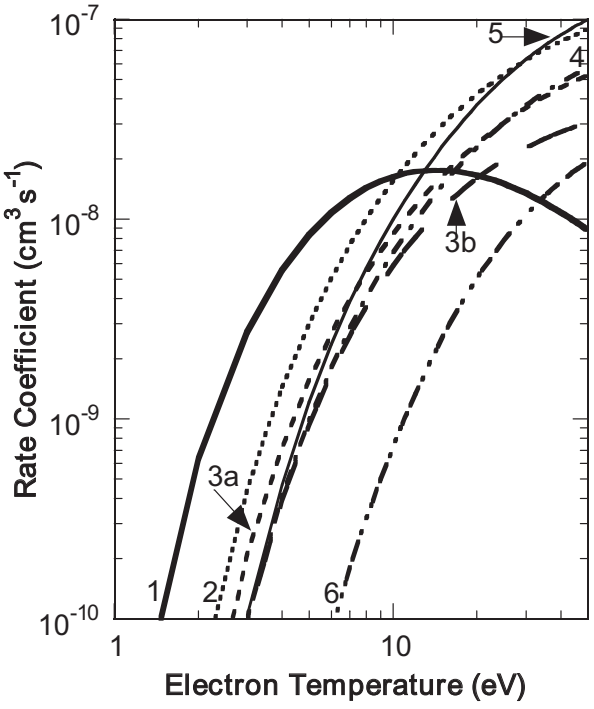

Figure 3. Rate coefficients for the competing processes in low temperature N_2 plasmas. The legend is the same as in figure 2.

where A_i is the atomic or molecular species density (cm^{-3}), n_e and n_{N_2} are the electron and nitrogen density, respectively, and $\langle \sigma \nu \rangle_i$ is the rate coefficient ($cm^3\,s^{-1}$) for any of the reactions described above. For reaction 4, the N_2 density in equation (1) must be replaced by the atomic density n_N. Since formation rates for every reaction (except 4) depend on the same $n_e \times n_{N_2}$ product, a simple comparison between rate coefficients identifies the dominant process. Rate coefficients for the different reactions at temperatures of 2, 5, 10, 15 and 20 eV are given in table 3. Examination of table 3 reveals that the molecular excitation process dominates at 2 and 5 eV but becomes smaller than the total dissociation process (16.3 compared to 15.6 + 8.49 + 5.87) at 10 eV. For T_e higher than 10 eV, excitation plays only a minor role in determining the dominant plasma species. If large GaN growth rates are indeed due to a large N_2 metastable population and a small N population, then the rate coefficients listed in table 3 suggest that for maximum GaN growth, helicon sources should be operated at low T_e where the excitation process is dominant. Hence, growth-detrimental reactions could be studied by operating the source at high T_e where N_2 dissociation dominates.

3.2. Excited N_2 states

To predict which N_2 excited states will be present near the substrate, we must consider the lifetimes and the excitation rate coefficients of the different excited levels. The nitrogen molecule has 27 tabulated primary levels with energies ranging from the ground state level $X\,^1\Sigma_g^+$ (0 eV) to the $z\,^1\Delta_g$ level at 14.30 eV [27]. A simplified energy diagram of the N_2 molecule is given in figure 4 [27, 29, 54]. The high energy levels (>12.5 eV) of the N_2 molecule as well as the septet term are omitted from figure 4. These high energy levels have small excitation cross-sections [31, 38] and molecule in those states are likely to quickly decay to lower energy states. Alternatively, these high energy states can also vanish by spontaneous dissociation since their energy is larger than dissociation threshold [27]. Quintet energy levels and lifetimes are taken from recent publications [55–57]. Each of the excited levels has a number of sub-levels associated with values taken by the inner quantum number J. The excitation rate coefficients for the different excited levels of the nitrogen molecule are calculated from electron impact cross-sections [38] using the same technique described earlier (see section 3.1). Three important transition arrays are also shown in figure 4. The first positive system (FPS) occurs between the $B\,^3\Pi_g$ and $A\,^3\Sigma_u^+$ states of the nitrogen molecule. The second positive system (SPS) occurs between the $C\,^3\Pi_u$ and $B\,^3\Pi_g$ levels. The first negative system (FNS) occurs

Table 3. Rate coefficients for competing reactions at 2, 5, 10, 15 and 20 eV.

T_e (eV)	$\langle \sigma \nu \rangle_1$ ($10^{-9}\,cm^3\,s^{-1}$)	$\langle \sigma \nu \rangle_{1a}$ ($10^{-9}\,cm^3\,s^{-1}$)	$\langle \sigma \nu \rangle_2$ ($10^{-9}\,cm^3\,s^{-1}$)	$\langle \sigma \nu \rangle_{3a}$ ($10^{-9}\,cm^3\,s^{-1}$)	$\langle \sigma \nu \rangle_{3b}$ ($10^{-9}\,cm^3\,s^{-1}$)	$\langle \sigma \nu \rangle_5$ ($10^{-9}\,cm^3\,s^{-1}$)	$\langle \sigma \nu \rangle_6$ ($10^{-9}\,cm^3\,s^{-1}$)
2	0.632	0.131	0.0479	0.0192	6.62 e−3	0.0104	1.22 e−5
5	8.36	1.27	3.02	1.57	0.935	1.21	3.39 e−2
10	16.3	2.39	15.6	8.49	5.87	10.0	0.734
15	17.6	2.45	29.6	16.4	11.3	23.1	2.55
20	16.6	2.31	42.3	23.8	16.0	37.3	5.09

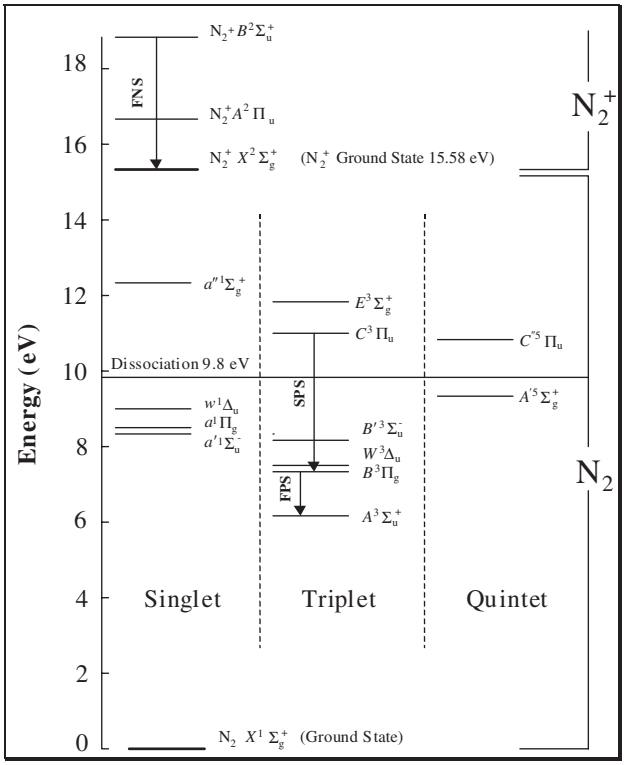

Figure 4. Simplified energy diagram of N_2 with molecular transitions (arrows) observed during experiments. Only the most prominent low energy levels of the N_2 molecule are shown (all the high energy levels (>12.5 eV) as well as the septet state are omitted). FPS, SPS and FNS transitions (arrows) stand for first positive, second positive and FNSs, respectively.

Table 4. Energy levels and lifetimes of some N_2 excited levels.

Level	Energy (eV)	Lifetimes (s)	Primary decay level
$A\,^3\Sigma_u^+$	6.167	1.27	$X\,^1\Sigma_g^+$
$B\,^3\Pi_g$	7.351	8.0×10^{-6}	$A\,^3\Sigma_u^+$
$W\,^3\Delta_u$	7.360	10^{-3}	$B\,^3\Pi_g$
$B'\,^3\Sigma_u^+$	8.163	4×10^{-6}	$B\,^3\Pi_g$
$a'\,^1\Sigma_u^-$	8.396	0.7	$X\,^1\Sigma_g^+$
$a\,^1\Pi_g$	8.547	1.7×10^{-4}	$X\,^1\Sigma_g^+$
$w\,^1\Delta_u$	8.887	2.5×10^{-4}	$a\,^1\Pi_g$
$A'\,^5\Sigma_g^+$	9.419	$(\approx10^{-11}, 4\times10^{-5})$*	$(B\,^3\Pi_g)$*
$C''\,^5\Pi_u$	10.72	4.3×10^{-6}	$A'\,^5\Sigma_g^+$
$C\,^3\Pi_u$	11.03	3.7×10^{-8}	$B\,^3\Pi_g$
$E\,^3\Sigma_g^+$	11.87	2.0×10^{-4}	$A\,^3\Sigma_u^+$
$a''\,^1\Sigma_g^+$	12.25	$<10^{-7}$	$X\,^1\Sigma_g^+$

* The rapid decay of the $A'\,^5\Sigma_g^+$ level is through the gateway mechanism. The transition $A'\,^5\Sigma_g^+ \rightarrow B\,^3\Pi_g$ is a fast radiationless transition ($\approx10^{-11}$ s) [60, 86]. Only an even number J level of the $A'\,^5\Sigma_g^+$ couples with $B\,^3\Pi_g$ sub-levels (see text). The overall lifetime of the metastable $A'\,^5\Sigma_g^+$ is 40 μs [57].

between the $B\,^2\Sigma_u^+$ and $X\,^2\Sigma_g^+$ states of the nitrogen molecular ion (N_2^+), the latter being the ground state of the molecular ion.

For the N_2 molecule, there are four important singlet levels: the metastable states $a'\,^1\Sigma_u^-$, and $a\,^1\Pi_g$, and the excited states $w\,^1\Delta_u$ and $a''\,^1\Sigma_g^+$. These levels are listed in table 4 with their respective energy levels, lifetimes and their primary decay levels [27, 58] (states to which the excited levels will preferentially decay, i.e. with the largest transition probability). The bottom singlet levels $a'\,^1\Sigma_u^-$, $a\,^1\Pi_g$ and $w\,^1\Delta_u$ are interconnected via the McFarlane infrared system [27]. Electron populations in higher singlet states will cascade down to enhance the population of these three levels.

The important triplet levels are the metastables $A\,^3\Sigma_u^+$ and $E\,^3\Sigma_g^+$, as well as the excited states: $B\,^3\Pi_g$, $B'\,^3\Sigma_u^+$, $W\,^3\Delta_u$ and $C\,^3\Pi_u$. The other high energy triplet levels ($D\,^3\Sigma_u^+$) have very small cross-sections and will quickly decay to lower energy singlet states. The energy levels, lifetimes [27, 58] and primary decay levels are shown in table 4. For the triplet states, the excited electron populations of all these high energy triplet levels will eventually decay to the $A\,^3\Sigma_u^+$ metastable level [27, 59]. Because of the long lifetime of the $A\,^3\Sigma_u^+$ state, neutral quenching and wall deactivation are important loss mechanisms for this metastable.

The sole known septet level $^7\Sigma_u^+$ (not observed [27]) is omitted in this paper because this level is generally believed to a repulsive state [55]. Thus, its formation cross-section and subsequent population will remain negligible under all plasma conditions investigated here. For quintet states, two levels are known: $A'\,^5\Sigma_g^+$ and $C''\,^5\Pi_u$. The first of these two levels is a metastable state while the second is an excited level that spontaneously decays towards the $A'\,^5\Sigma_g^+$ state emitting the Herman infrared bands (HIR) [54]. The decay of the $A'\,^5\Sigma_g^+$ is more complicated since it occurs through a 'gateway mechanism' [57, 60–63] to reach the $B\,^3\Pi_g$ and eventually the $A\,^3\Sigma_u^+$ via the FPS. The decay from the $A'\,^5\Sigma_g^+$ level to the $B\,^3\Pi_g$ state is believed to be a fast process through a radiationless transition [61, 63]. According to this mechanism, the collisions scramble only the levels within the $A'\,^5\Sigma_g^+$ state, while the $A'\,^5\Sigma_g^+ \rightarrow B\,^3\Pi_g$ transition occurs spontaneously through spin–orbit (S/O) coupling. These radiationless transitions occur between the $A'\,^5\Sigma_g^+$ sub-levels ($v = 0, 2, 4$) and the $B\,^3\Pi_g$ ($v = 10, 11, 12$) and significantly enhance the electron population of these three $B\,^3\Pi_g$ sub-levels [55, 62, 63]. Consequently, transitions originating from these sub-levels with the largest Einstein coefficients are the new dominant transitions of the FPS [64]. With this quintet contribution, the $B\,^3\Pi_g \rightarrow A\,^3\Sigma_u^+$ (10–6), (11–7) and (12–8) transitions with band head, respectively, located at 585.4 nm, 580.4 nm and 575.5 nm [27] become the dominant transitions of the FPS. This population transfer between the quintet and triplet manifolds is likely responsible for the bright orange colour observed in the plasma core at high pressure [65].

No excitation cross-section for both quintet states could be found in the literature (the $A\,^5\Sigma_g^+$ can only be detected indirectly). Previously believed to be very shallow [27], the depth of the $A\,^5\Sigma_g^+$ potential well is now estimated at 0.4 eV below dissociation [57]. Thus, significant electron population can be excited to this state in moderate temperature plasmas. The relative importance of the $A'\,^5\Sigma_g^+$ population is unknown. However, since most of the $A\,^5\Sigma_g^+$population ends up as $B\,^3\Pi_g$ and eventually as $A\,^3\Sigma_u^+$, the $A'\,^5\Sigma_g^+$ can ultimately be considered as another highly excited triplet state.

Based on the above analysis, the most likely distribution of the metastable states in low temperature N_2 plasmas is

as follows. Because of the large excitation rate coefficients for the $B\,^3\Pi_g$, $W\,^3\Delta_u$, $C\,^3\Pi_u$ and $A\,^3\Sigma_u^+$ triplet states and the inevitable decay of these three first levels toward the $A\,^3\Sigma_u^+$ metastable, the $A\,^3\Sigma_u^+$ state will likely be the dominant metastable in the plasma. Adding to the population of the $A\,^3\Sigma_u^+$ state are contributions from the quintet states via the 'gateway mechanism' described above. To evaluate the $A\,^3\Sigma_u^+$ metastable density in the vicinity of the substrate, the sum of the excitation rate coefficients of all triplet states must be considered. At low T_e, the sum of all excitation rate coefficient predict that more than 70% of the total excited species should be triplet states with a significant percentage in the metastable state $A\,^3\Sigma_u^+$. Since interconnection between singlet and triplet states is forbidden, a significant number of singlet metastables are also likely to be present in the plasma. The dominant singlet metastable is harder to identify because of the interconnection of the three lowest singlet levels via the McFarlane system. Because of its longer lifetime, the $a'\,^1\Sigma_u^-$ metastable will likely be the dominant singlet metastable. Because of its large excitation rate coefficient, the singlet $a\,^1\Pi_g$ metastable state should also be present in the plasma.

4. Experiments

To investigate the possibility for control of the N_2 reactive species in a helicon source, we performed a series of experiments for a range of operating pressures in HELIX. All of the other parameters, RF power, RF frequency, magnetic field and antenna configuration were kept constant during the experiments. The plasma parameters were 600 W, 9 MHz and 600 Gauss with a fractional helical antenna configuration, respectively. The filling pressure was varied from 0.14 to 8 mTorr. Both T_e and n_e change as a function of pressure. At low pressure (0.2 mTorr), the whitish purple N_2 plasma (bright white core surrounded by a purplish annulus) is characterized by a low density and a moderate T_e ($\approx 5 \times 10^{11}$ cm^{-3}, 16 eV), while at high pressure (8 mTorr), the pinkish orange plasma (bright orange core surrounded by a pinkish annulus) has a higher density and a lower temperature ($\approx 5 \times 10^{12}$ cm^{-3}, 4 eV). A similar T_e dependence on pressure was observed in helium plasmas during development of a He line ratio diagnostic to measure T_e [16]. The spectroscopy diagnostic, described briefly in section 2, was used to monitor five different nitrogen species in the plasma, namely: N II (atomic ion), N I (atomic neutral), N_2^+ (molecular ion) and two different excited states of the N_2 molecule as a function of the filling pressure. The integrated line or band intensity for each of these species is normalized to its respective maximum value and shown in figure 5 as a function of the pressure.

The N II ($3P^1D \rightarrow 3S^1P^o$; 399.5 nm) singlet line is the brightest transition of the atomic nitrogen ion emission spectrum [66, 67]. The line intensity is very weak at high pressure and reaches modest intensity levels at low pressure. This suggests that very few atomic ions are present in the plasma even at low pressure. At high pressure, the line intensity is difficult to evaluate since the N_2 ($C\,^3\Pi_u$, $\nu' = 1 \rightarrow B\,^3\Pi_g$, $\nu'' = 4$ at 399.8 nm) molecular band is present in the same spectral region [27]. We believe that the N II line intensity at high pressure is even smaller than what is shown in figure 5. The line intensity peaks at 0.3 mTorr and

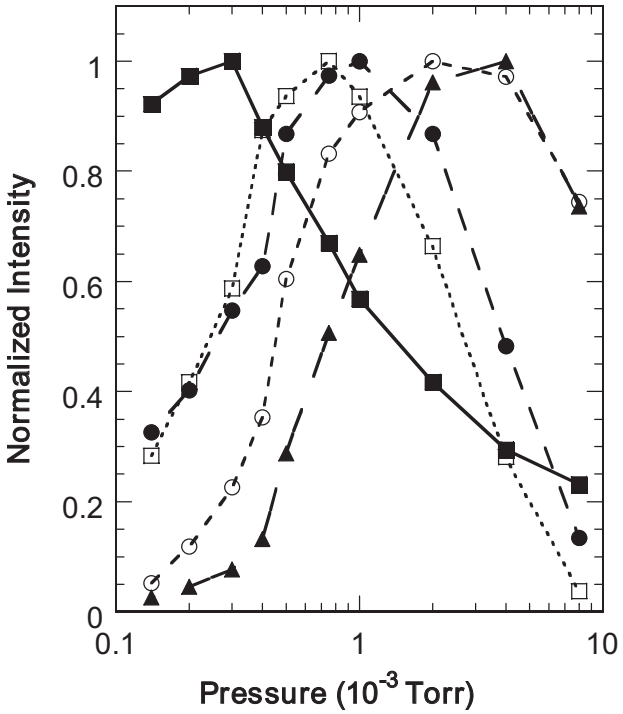

Figure 5. Normalized line intensities of the different nitrogen species found in the plasma. Lines between points are solely guides to the eye. N II (■), N I (□), N_2^+ (●), N_2^* ($C\,^3\Pi_u \rightarrow B\,^3\Pi_g$) (○), N_2^* ($B\,^3\Pi_g \rightarrow A\,^3\Sigma_u^+$) (▲).

then slowly decreases as a function of increasing pressure. These observations are consistent with decreasing T_e as a function of pressure. The recombination rate coefficient of N II ($\approx 2.1 \times 10^{-11}$ cm^3 s^{-1}) [68] remains small when compared to the formation rate coefficient (see figure 3) for all pressures used in this experiment. This suggests that charge exchange (with N_2) is the dominant loss mechanism for this nitrogen ion.

The N I ($3P^4D^o \rightarrow 3S^4P$; 868.0 nm) quartet line is among the brightest transitions of the atomic nitrogen spectrum [66, 67]. This transition has been used previously to monitor the presence of atomic nitrogen in a plasma [69]. This line is intense at low to moderate pressure (0.14–0.75 mTorr, see figure 6(*a*)) but fades at higher pressure. At high pressure, the N I line is completely dominated by the presence of strong emission bands associated with the N_2 molecule (see figure 6(*b*)). In figures 6(*a*) and (*b*), the spectral region centred on 868 nm is shown under two different plasma conditions. In figure 6(*a*) the pressure is set at 1.4×10^{-4} Torr while in figure 6(*b*) the pressure is set at 8.0×10^{-3} Torr. Spectrometer settings and all other plasma parameters are kept constant. In figure 6(*a*), three lines from the $3P^4D^o \rightarrow 3S^4P$ quartet transition array are clearly visible at 868.03, 868.33 and 868.61 nm [70]. The head of two molecular bands are barely perceptible at 867.6 and 869.1 nm. Note that these weak bands could alternatively originate from the colder outer plasma instead of the core since the optics used for spectroscopy optics collect radiation along a line-of-sight through the entire plasma column [71]. In figure 6(*b*), the atomic lines vanish into the sea of more intense molecular bands. The molecular transitions are secondary bands of the FPS ($B\,^3\Pi_g \rightarrow A\,^3\Sigma_u^+$) [27]. The absence of atomic emission at 868.33 nm (see figure 6(*b*))

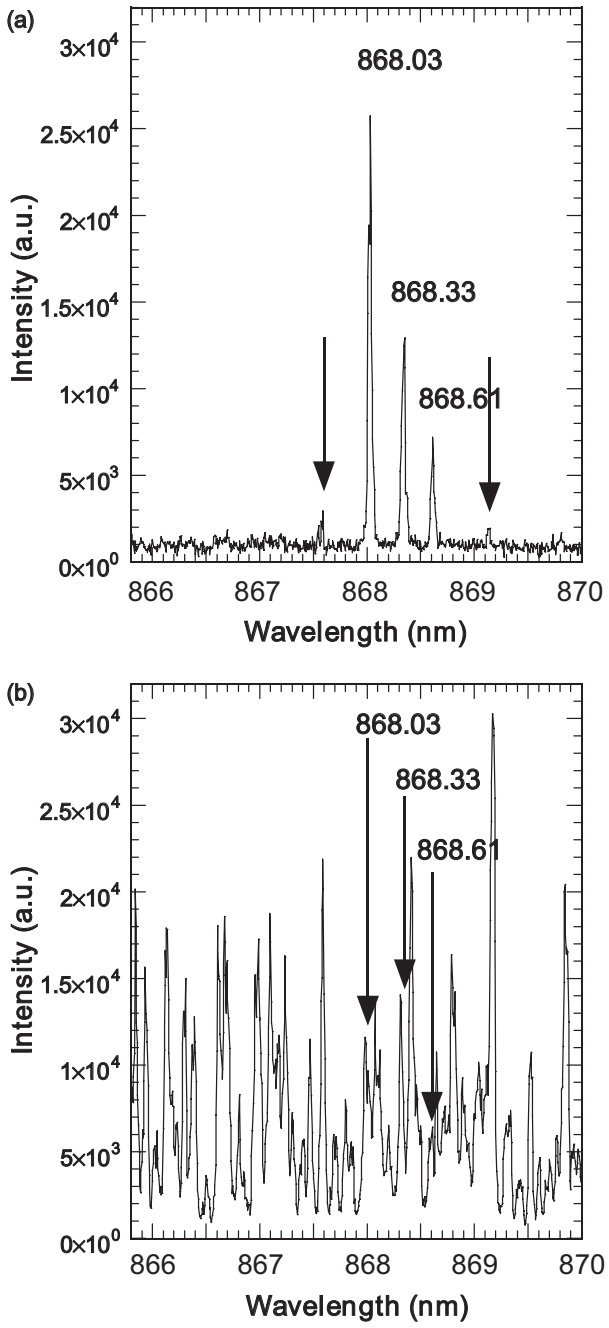

Figure 6. (*a*) 868.0 nm spectral region at 1.4×10^{-4} Torr. The three lines are part of the $3P^4D^o \rightarrow 3S^4P$ quartet transition array. The N I atomic transitions are at 868.03 nm ($3P^4D^o_{7/2} \rightarrow 3S^4P_{5/2}$), 868.33 nm ($3P^4D^o_{5/2} \rightarrow 3S^4P_{3/2}$) and 868.61 nm ($3P^4D^o_{5/2} \rightarrow 3S^4P_{3/2}$), respectively. The arrows indicate the head of two very weak molecular bands at 867.59 and 869.18 nm. (*b*) 868.0 nm spectral region at 8.0×10^{-3} Torr. The spectrum is covered with secondary molecular bands of the FPS ($B\,^3\Pi_g \rightarrow A\,^3\Sigma^+_u$). The arrows indicate the location of the three dominant atomic lines seen in figure 6(*a*).

suggests that atomic radiation is very weak at high neutral pressure. From figures 6(*a*) to (*b*), a significant transformation of the plasma from an atomic to a molecular nature has taken place.

Other transitions involving doublet states such as N(^{2}P) or N(^{2}D) are very weak even under low pressure operation. This reflects the fact that formation rate coefficients for quartet states are much larger than the formation rate coefficients for doublet states. Just in terms of the three states N(^{4}S) N(^{2}P) or N(^{2}D) listed in table 2, the model predicts that the population of the N(^{4}S) state is always at least five times larger than the population of the N(^{2}D) and N(^{2}P) states for $T_e \geqslant 5$ eV. In reality, the situation is even more skewed toward the formation of quartet states. In our experiments, the quartet transitions were at least 100 times more intense than any doublet transitions. This indicates that direct production of excited quartet levels via dissociative excitation (reaction 3, table 2) is highly probable when T_e becomes large. The rate coefficient for dissociative excitation involving higher excited quartet states is probably much larger than the corresponding process involving doublet levels. Other research groups have observed that the concentrations of doublet metastable states are several orders of magnitude smaller than the density of N(^{4}S) [72]. Since the lifetimes of the nitrogen ground state N(^{4}S) and the metastables atomic states N(^{2}P) and N(^{2}D) in high density, low temperature plasmas are several hours [72–74], it is likely that wall recombination is the dominant atomic loss process in our experiment. The absence of molecular bands (associated with recombination) at low pressure where the density of N(^{4}S) is large confirms this hypothesis.

The N_2^+ ($B\,^2\Sigma^+_u,\ \nu' = 0 \rightarrow X\,^2\Sigma^+_g,\ \nu'' = 1$ at 427.8 nm) transition is part of the FNS band from the $B\,^2\Sigma^+_u$ excited level to the ground state $X\,^2\Sigma^+_g$ of the nitrogen molecular ion (see figure 4) [27, 75]. This N_2^+ band reached maximum intensity at 1.0 mTorr. Although this band was present for every pressure, the intensity at both extremities of the experimental pressure range was weak compared to the maximal central value. According to table 3, molecular ionization by electron impact should be important for $T_e >$ 10 eV. In our experiment, 10 eV temperatures are observed when the pressure is close to 1 mTorr. For lower pressure, the dominant process is molecular dissociation (see table 3). The steady decrease of intensity of the N_2^+ band with falling pressure can thus be explained in terms of a combination of two factors: (1) the decrease of the number of N_2 molecules in the discharge; (2) the increasing fraction of N_2 molecules that are dissociated instead of ionized in the plasma. In the other direction (higher pressure) the trend is towards excitation instead of molecular ionization and the decline in intensity of the N_2^+ band reflects this situation. The recombination picture for N_2^+ is unclear. Electron impact recombination has a very low rate coefficient in plasma conditions described here and is highly unlikely [76]. Dissociative recombination through N_4^+ formation [77, 78] ($N_2^+ + N_2 \rightarrow N_4^+$; $N_4^+ + e^- \rightarrow 2N_2$) has a much larger rate coefficient and is probably the dominant process. Simple dissociative recombination [40, 77, 78] is also possible ($N_2^+ + e^- \rightarrow N + N$) under these plasma conditions. Because N_2^+ is confined by the magnetic field, wall neutralization is not believed to be important. Additional work is needed to determine the relative importance of each of the recombination processes for N_2^+.

The N_2 ($C\,^3\Pi_u,\ \nu' = 0 \rightarrow B\,^3\Pi_g,\ \nu'' = 0$) transition at 337.1 nm corresponds to the fundamental transition band (0–0) of the SPS between the two excited levels $C\,^3\Pi_u$ and $B\,^3\Pi_g$ of the nitrogen molecule (see figure 4) [27]. This N_2 band is very weak at low pressure, reaches maximum intensity

at 2.0 mTorr, and slowly decreases towards higher pressure. The N_2 ($B\,^3\Pi_g$, $\nu' = 11 \rightarrow A\,^3\Sigma_u^+$, $\nu'' = 7$) transition at 580.4 nm is part of (FPS) between the two excited levels $B\,^3\Pi_g$ and $A\,^3\Sigma_u^+$ of the nitrogen molecule [75] (see figure 4). This band is very weak at low pressure and becomes dominant at high pressure with a maximum intensity at 4.0 mTorr. As expected, these two N_2 transitions have a similar behaviour as a function of pressure. However, the band originating from the high energy level ($C\,^3\Pi_u$) reaches its maximum at a lower pressure than the other neutral molecular band. This behaviour is consistent with decreasing T_e as a function of increasing pressure. The small decrease at 8 mTorr is related to the fact that the excitation rate coefficient becomes smaller as T_e drops below 5 eV (see table 3). At high pressure ($\geqslant$4 mTorr) a bright orange core is observed. The plasma core light intensity increases with pressure. This intense radiation is directly linked to strong molecular bands observed around 580 nm (band heads at 585.4, 580.4 and 575.5 nm). These observations combined with the very weak concentration of atomic species in the plasma (decreasing T_e with pressure) lead us to believe that atomic recombination as little to do with the intense molecular de-excitation [65, 79]. Clearly, decay of triplet (and quintet via the gateway mechanism) excited states occurs first and foremost via strong transitions such as the FPS and the SPS arrays. Neutral quenching [79–81] in the outer plasma (and in the neutral gas surrounding the plasma) together with wall deactivation [72, 82–84] are the two other important loss mechanisms for the excited N_2 species. The intense molecular bands associated the FPS (and SPS) observed in the helicon plasma, combined with the long lifetime of the $A\,^3\Sigma_u^+$ metastable [27], lead us to conclude that a significant $A\,^3\Sigma_u^+$ population is likely present in the plasma at 4 and 8 mTorr.

5. Discussion

Under the plasma conditions used in this study, the plasma emission spectrum changes from an almost purely atomic nature at low pressure to a highly molecular nature at high pressure. At low pressure, little or no molecular emission is observed and the plasma is essentially atomic. All processes associated with high T_e, such as dissociative ionization and dissociative excitation are observed at low neutral pressure. The process of ionization plus excitation of the nitrogen molecule is observed in the middle of the pressure range, and all processes related to excitation and de-excitation of N_2 are observed at high pressure. The line intensity profiles shown in figure 5 are consistent with decreasing T_e as a function of increasing pressure. These observations agree well with the comparison of the formation rates presented in table 3. By going from high to low pressure, the order in which the different N_2 species reached their respective maximum is the same as the one predicted by the different excitation rate coefficients with increasing temperature. The fact that the dominant species is changing as a function of pressure also indicates that the crucial parameter is T_e and not n_e. According to equation (1), for constant temperature plasma, only the line intensity would vary as a function of n_e, not the chemistry. Thus, an important method of controlling the chemistry of the N_2 plasma is to vary the T_e. Similar observations were made by a different research group using a compact electron cyclotron resonance (ECR) microwave plasma source [85]. However, unlike our source, their source produced a mix of atomic and molecular species under all plasma conditions presented in their paper. Nevertheless, it is interesting to note that they observed a comparable transformation in the nature of their plasma (primarily molecular to mostly atomic) just by reducing the filling pressure. Also of great interest is the fact that they were able to increase, to a lesser extent, the atomic nature of the plasma by increasing the RF power of the source. We suggest that these observations are consistent with increasing T_e as a function of decreasing pressure and increasing RF power, respectively.

Our experiments employed only one of the potential 'dials' to change the active species in N_2 helicon plasmas. A more aggressive approach using a combination of different parameters would allow us to further extend the T_e range, thus enabling precise selection of a specific species for GaN growth investigation. This technique of using a combination of source parameter changes to control the T_e has been successfully used in helium helicon plasma [16]. In those experiments, electron temperatures between 3 and 20 eV were obtained by varying pressure, RF power, magnetic field and RF frequency in He plasmas. A comparable temperature range can easily be achieved for N_2 plasma. Moreover, extension of the operating pressure range in the source beyond minimum and maximum values used in this first study can be accomplished without major difficulties. Also suggested by this study, is that selection within identical species of different excited states might be possible. The fact that the maximum intensity of the $C\,^3\Pi_u \rightarrow B\,^3\Pi_g$ transition was observed at a different pressure than the $B\,^3\Pi_g \rightarrow A\,^3\Sigma_u^+$ transition, indicates that the plasma could ultimately be fine-tuned to produce a given species with a specific excited state.

Our study shows that the production of nitrogen plasmas dominated by atomic species is clearly feasible. As for molecular plasmas, a reduction in the RF power would significantly reduce the T_e and bring us even closer to a purely molecular plasma. These conclusions are consistent with the rate coefficients for the competing processes in low temperature plasma given earlier in table 3. In both plasma regimes, it could be possible to improve on the 'purity' of the plasma by adjusting other parameters such as the magnetic field and the RF frequency.

Finally, the assumption that the electron velocity distribution in these helicon source plasmas can be effectively described by Maxwellian distribution for analysis purposes is validated. The clear transition from atomic to molecular plasma is incompatible with a dual electron temperature distribution.

6. Conclusion

The different nitrogen species that can be found in nitrogen helicon plasmas are identified. The competing plasma processes involved in the creation of these species are also described with special emphasis on the excitation processes responsible for the formation of N_2 metastables in the plasma. Our study shows that the line intensity variations as a function of augmenting pressure are consistent with decreasing T_e. These observations agree well with the comparison of the

formation rates derived from the literature. The crucial parameter for control of the plasma chemistry is shown to be the electron temperature. This study suggests that the production of almost purely atomic nitrogen plasma or purely molecular nitrogen plasma is possible in a helicon plasma source.

References

[1] Morkoc H *et al* 1994 *J. Appl. Phys.* **76** 1363
[2] Pearton S J *et al* 1999 *J. Appl. Phys.* **86** 1
[3] Jain S C *et al* 2000 *J. Appl. Phys.* **87** 965
[4] Kim K *et al* 1995 *J. Vac. Sci. Technol.* B **12** 796
[5] Kumar S 1996 *MS Thesis in Chemical Engineering* West Virginia University, Morgantown
[6] Myers T H *et al* 1998 *J. Vac. Sci. Technol.* B **16** 2261
[7] Myers T H *et al* 1999 *J. Vac. Sci. Technol.* B **17** 1654
[8] Ptak A J *et al* 1999 *Appl. Phys. Lett*. **74** 3836
[9] Newman N 1997 *J. Cryst. Growth* **178** 102
[10] Keiter P A, Scime E E and Balkey M M 1997 *Phys. Plasmas* **4** 2741
[11] Watari T *et al* 1978 *Phys. Fluids* **21** 2076
[12] Boswell R W 1970 *Phys. Lett.* A **33** 457
[13] Shoji T *et al* 1993 *Plasma Sources Sci. Technol*. **2** 5
[14] Degeling A W and Boswell R W 1998 *Phys. Plasmas* **4** 2748
[15] Chen F F and Blackwell D D 1999 *Phys. Rev. Lett*. **82** 2677
[16] Boivin R F, Kline J L and Scime E E 2001 *Phys. Plasmas* **8** 5303
[17] Sudit I D and Chen F F 1994 *Plasma Sources Sci. Technol*. **3** 162
[18] Scime E E *et al* 1998 *Plasma Sources Sci. Technol*. **7** 186
[19] Scime E E *et al* 2001 *Rev. Sci. Instrum*. **72** 1672
[20] Godiak V A, Piejak R B and Alexandrovich B M 1993 *J. Appl. Phys*. **73** 3657
[21] Chen F F 1965 *Plasma Diagnostics* (New York: Academic)
[22] Kline K L *et al* 1999 *Phys. Plasmas* **6** 4767
[23] Keiter P A *et al* 2000 *Phys. Plasmas* **7** 779
[24] Scime E E *et al* 2000 *Phys. Plasmas* **7** 2157
[25] Balkey M M *et al* 2001 *Plasma Sources Sci. Technol.* **10** 284
[26] Allen J E, Boyd R L and Reynolds P 1957 *Proc. Phys. Soc.* B **70** 297
[27] Lofthus A and Krupenie P H 1977 *J. Phys. Chem. Ref. Data* **6** 113
[28] Wright A N and Winkler C A 1968 *Active Nitrogen* (New York: Academic)
[29] Schulz G J 1973 *Resonances in Electron Impact on Diatomic Molecules* NSRDS-NBS, vol 50 p 67
[30] Trajmar S, Register D F and Chutjan A 1983 *Phys. Rep*. **97** 219
[31] Trajmar S and Cartwright D C 1984 *Electron Molecule Interaction and their Application* ed L G Christophorou (New York: Academic)
[32] Zipf E C 1984 *Electron Molecule Interaction and their Application* ed L G Christophorou (New York: Academic)
[33] Herzberg G 1950 *Molecular Spectra and Molecular Structure V1* (Princeton, NJ: Van Nostrand-Reinhold)
[34] Rosenstock H M *et al* 1977 *J. Phys. Chem. Ref. Data* **6** (Suppl. 1) I-215–7
[35] Moore C E 1970 *Ionization Potentials and Ionization Limits Derived from the Analyses of Optical Spectra* NSRDS-NBS, vol 34
[36] Boivin R F and Scime E E 2003 *Rev. Sci. Instrum.* **74** 4352
[37] Keesee A M, Scime E E and Boivin R F 2004 *Rev. Sci. Instrum.* **75** 4091
[38] Cartwright D C *et al* 1977 *Phys. Rev*. A **16** 1041
[39] Winters H F 1966 *J. Chem. Phys*. **44** 1472
[40] Zipf E C, Epsy P J and Boyle C F 1980 *J. Geophys. Res.* **85** 687
[41] Zipf E C and McLauglin R W 1978 *Planet. Space Sci*. **26** 449
[42] Barnet C F *et al* 1977 *Atomic Data for Controlled Fusion Research* ORNL-5207
[43] Tawara H and Kato T 1987 *At. Data Nucl. Data Tables* **36** 167
[44] Zhu P and Boswell R W 1991 *Phys. Fluids* B **3** 869
[45] Chen F F 1991 *Plasma Phys. Control. Fusion* **33** 339
[46] Chen F F and Decker C D 1992 *Plasma Phys. Control. Fusion* **34** 635
[47] Ellingboe A R *et al* 1995 *Phys. Plasmas* **2** 1807
[48] Molvik A W, Ellingboe A R and Rognlien T D 1997 *Phys. Rev. Lett*. **79** 233
[49] Chen R T S and Hershkowitz N 1998 *Phys. Rev. Lett*. **80** 4677
[50] Scharer J, Degeling A, Borg G and Boswell R 2002 *Phys. Plasmas* **9** 3734
[51] Blackwell D D and Chen F F 1997 *Plasma Sources Sci. Technol.* **6** 569
[52] Chen F F and Blackwell D D 1999 *Phys. Rev. Lett.* **82** 2677
[53] Elton R C 1970 *Plasma Physics* (part A) (New York: Academic)
[54] Steinfeld J I 1985 *An Introduction to Modern Molecular Spectroscopy* 2nd edn (Cambridge, MA: MIT Press)
[55] Partridge H *et al* 1988 *J. Chem. Phys*. **88** 3174
[56] Ottinger C and Vilesov A F 1993 *Chem. Phys. Lett*. **211** 175
[57] Ottinger C and Vilesov A F 1994 *J. Chem. Phys*. **100** 4862
[58] Rundel R D and Stebbings R F 1972 *Case Studies in Atomic Collision Physics* vol II, ed E W McDaniel and M R C McDowell (Amsterdam: North-Holland)
[59] Borst W L and Chang S L 1973 *J. Chem. Phys*. **59** 5830
[60] Geisen H, Neuschäfer D and Ottinger C 1990 *J. Chem. Phys*. **92** 104
[61] Ottinger C, Smirnova L G and Vilesov A F 1994 *J. Chem. Phys*. **100** 7
[62] Morrill J S and Benesch W M 1994 *J. Chem. Phys*. **101** 6529
[63] Ottinger C and Vilesov A F 1994 *J. Chem. Phys*. **100** 4848
[64] Werner H J *et al* 1984 *J. Chem. Phys*. **81** 2420
[65] DeBenedictis S, Dilecce G and Simek M 1999 *J. Chem. Phys*. **110** 2947
[66] Lide D R 1993 *CRC Handbook of Chemistry and Physics* 74th edn (Boca Raton, FL: CRC Press)
[67] Chamberlain J W 1961 *Physics of the Aurora and Airglow* (New York: Academic)
[68] Nahar S N and Pradhan A K 1997 *Astrophys. J.* **111** (Suppl.) 339
[69] Bischel W K, Perry B E and Crosley D R 1981 *Chem. Phys. Lett*. **82** 85
[70] Wiese W L, Smith M W and Glennon B M 1966 *Atomic Transitions Probabilities* vol 1, National Standard Reference Data System, NSRDS-NBS–4
[71] DeSilva A W and Goldenbaum G C 1970 *Plasma Physics* (part A) chapter 3, ed H R Griem and R H Lovberg (New York: Academic)
[72] Pejović M M *et al* 2002 *J. Phys*. **35** 2536
[73] Black G *et al* 1969 *J. Chem. Phys*. **51** 116
[74] Lin C H and Kaufman F 1971 *J. Chem. Phys*. **55** 3760
[75] Pearse R W B and Gaydon A G 1963 *The Identification of Molecular Spectra* (New York: Wiley)
[76] Massey H S W and Gilbody H B 1974 *Electronic and Ionic Impact Phenomena* vol IV (Oxford: Clarendon)
[77] Hamilton D H 1973 *J. Chem. Phys*. **58** 4820
[78] Kossyi I A *et al* 1992 *Plasma Sources Sci. Technol.* **1** 207
[79] Piper L G 1989 *J. Chem. Phys.* **91** 864
[80] Sa P A and Loureiro L J 1997 *J. Phys. D: Appl. Phys.* **30** 2320
[81] Guerra V and Loureiro L J 1997 *Plasma Sources Sci. Technol.* **6** 361
[82] Black G *et al* 1974 *J. Chem. Phys.* **60** 116
[83] Pillow M E and Rogers A J 1963 *Proc. Phys. Soc.* **81** 1034
[84] Boisse-Laporte C, Chave-Normand C and Marec J 1997 *Plasma Sources Sci. Technol.* **6** 70
[85] Vaudo R P, Cook J W Jr and Schetzina J F 1994 *J. Vac. Sci. Technol.* B **12** 1232
[86] Siegbahn P E 1983 *Int. J. Quantum Chem.* **23** 1869